UCRL-92305
PREPRINT

On the Free Vibrations of Some Viscoelastic Solids

R.C.Y. Chin
G.W. Hedstrom
G. Mayeda

The revision of this paper was published in the
Geophysical Journal/Royal Astronomical Society
Volume 86, pages 137-166

March 6, 1985

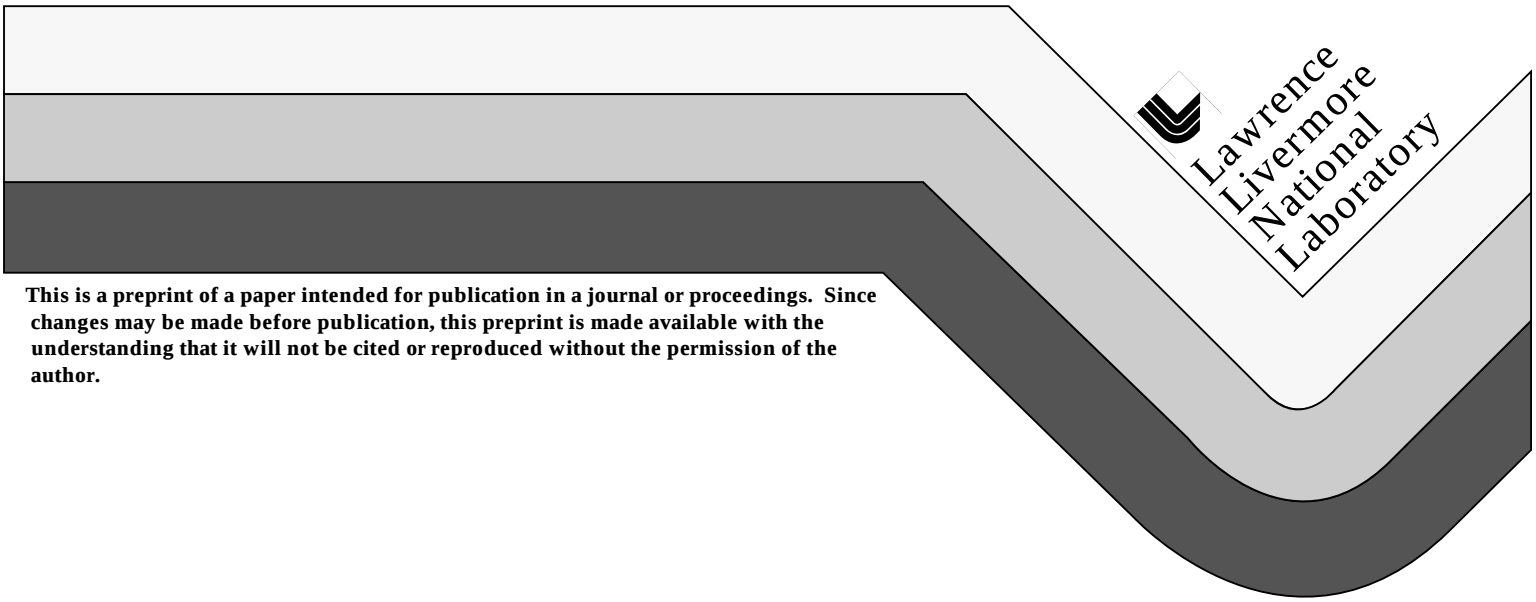

Work performed under the auspices of the U.S. Department of Energy by Lawrence Livermore National Laboratory under Contract W-7405-ENG-48.

On the Free Vibrations of Some Viscoelastic Solids

by

R. C. Y. Chin and G. W. Hedstrom

Lawrence Livermore National Laboratory
P. O. Box 808, Livermore, California 94550

and G. Majda

Division of Applied Mathematics, Brown University
Providence, Rhode Island 02912

Summary. In this study we apply the correspondence principle for free vibrations of a homogeneous viscoelastic solid derived by Fisher and Leitman to obtain the torsional modes of a homogeneous viscoelastic rod. We also extend the correspondence principle, showing that it may be used to find the frequencies of Love waves in a stratified viscoelastic medium. Finally, we apply the correspondence principle to four viscoelastic materials: the Kelvin-Voigt solid, the Maxwell solid, the standard linear solid, and the Achenbach-Chao solid. We show that in each of these cases some care must be used in applying the correspondence principle because of the presence of multiple solutions.

1 Introduction

In this study we are concerned with some problems in viscoelastic wave propagation. Viscoelastic media are of geophysical interest because Spencer (1981) has found that they model fully saturated porous rocks. In addition, the experiments of Bonner (reported in (Thigpen *et al.* 1983)) show that a partially melted granitic rock is modelled by a viscoelastic material. An understanding of wave propagation processes in fully or partially saturated porous materials is basic to energy resource recovery, geothermal exploration, and resource assessment. In addition, in solid earth geophysics the study of attenuation and dispersion of seismic waves involves the theory of linear viscoelasticity. In particular, the damping of the free oscillations of the earth, i. e., the quality factor Q is a topic of considerable interest. The aim of this study is to increase our understanding of viscoelastic wave propagation with a view toward applications in the analysis of attenuation and dispersion in geophysical materials.

For the elastic wave equation consider solutions of the form of sinusoidal waves $f(\mathbf{x})\exp(i\omega_e t)$. Then the amplitude f of the displacement field satisfies a differential equation which is formally self-adjoint (Achenbach 1975), and the frequency ω_e is an eigenvalue. Thus, if the problem is on a bounded domain with Dirichlet, Neumann, or Robin boundary conditions, the problem as a whole is self-adjoint and the eigenvalues are real and the spectrum has no continuous component. If, on the other hand, the domain is unbounded and the Sommerfeld radiation condition is used on part of the boundary, then the problem as a whole is not self-adjoint, so that the spectrum may have one or more continuous components. Even in this case, though, the discrete spectrum is strictly real.

For wave propagation in a viscoelastic medium and sinusoidal solutions $f(\mathbf{x})\exp(i\omega_v t)$ the differential equation for the amplitude f is not formally self-

adjoint. Therefore, even on a bounded domain the viscoelastic wave operator may have continuous components (Naimark 1968). Furthermore, the discrete eigenvalues ω_v need not be real. For realistic viscoelastic models in which the time-domain creep relaxation function is strictly real, the discrete eigenvalues appear in pairs,

$$\omega_v = \pm \mu + ib$$

with $\mu > 0$ and $b > 0$. The continuous spectrum arises as a result of the viscoelastic constitutive relation, and therefore, the structure and location of the continuous spectrum are model dependent. It should also be noted that for a viscoelastic wave problem in an unbounded domain the Sommerfeld radiation condition must be recast in terms of a projection onto the subspace of outgoing viscoelastic waves.

Starting from a known solution for the motion of an elastic material, there are two standard methods for analyzing wave motion in a corresponding viscoelastic media. One method is by perturbation from an elastic material to a nearby viscoelastic material. This has been done by several authors, and a careful analysis of the method was given by Majda *et al.* (1985), based on perturbation theory for linear operators (Kato 1966). They found that the validity of the procedure of perturbing elastic modes to obtain viscoelastic modes is highly model dependent. Furthermore, the size of perturbation permitted depends on the frequency and is limited by the distances separating modes. Other than the need to keep eigenvalues separated, the method gives no insight into the reasons for the restrictions.

The other method of analysis is based on the correspondence principle of Fisher & Leitman (1966). This principle says that for simple free vibrations of a homogeneous medium the displacement field $f(\mathbf{x})\exp(i\omega_v t)$ of a viscoelastic solid is related to the elastic displacement field $f(\mathbf{x})\exp(i\omega_e t)$ according to the conditions that the viscoelastic vibration frequency ω_v and the corresponding elastic frequency ω_e be related by the condition

$$\frac{\omega_v}{\omega_e} = \frac{K_v}{K_e}, \tag{1.1}$$

where K_v is the complex wave velocity and K_e is the corresponding real elastic wave velocity. That is, in terms of the elastic modulus M_e and the density ρ, we have $K_e = \sqrt{M_e/\rho}$. The viscoelastic wave speed $K_v = \sqrt{M_v(\omega_v)/\rho}$, depends on the frequency ω_v, and it is complex, because the viscoelastic material modulus M_v is complex. The correspondence principle of Fisher and Leitman says nothing about what happens to the continuous part of the spectrum for the elastic problem and it gives no information about any new continuous spectrum which may be present in the viscoelastic case but not in the elastic case. It should be noted that if (1.1) is regarded as a mapping from ω_e to ω_v, there may be more than one branch, and we have to use additional physical principles to select the proper branch.

In this paper we apply the correspondence principle (1.1) of Fisher & Leitman (1966) to the torsional modes of a viscoelastic rod and to viscoelastic Love waves in a stratified medium. In the case of Love wave this is actually an extension of the theory because we remove the restriction that the medium be homogeneous. The motivation for studying these two problems is that we can observe Love waves on seismograms and we can do laboratory experiments on rods. The theory presented here is needed as background information in the interpretation of the results. For this reason we find the location of the discrete spectrum for four different viscoelastic materials a Kelvin-Voigt solid (Leitman & Fisher 1973), a Maxwell solid (Leitman & Fisher 1973), a standard linear solid (Leitman

& Fisher 1973), and an Achenbach-Chao model solid (Achenbach & Chao 1962). We show that for each of these solids Eq. (1.1), regarded as an equation for ω_v, requires the introduction of a Riemann surface of at least two sheets. We use the our knowledge of the high- and low-frequency behavior of the spectrum to identify the principal sheet. The structure of the sheets determines the location of branch cuts joining them. The corresponding branch points form natural barriers for a perturbation expansion. We expect the branch cuts to give rise to components of continuous spectrum which have no analogue in the elastic medium. It happens also that for the Achenbach-Chao model solid for a range of values of the parameter, we must introduce still another branch cut because it is impossible to find a single sheet with both the proper high- and low-frequency behavior of the spectrum. A complete discussion of the continuous spectrum is more easily carried out from an analysis of the solution of a dynamic problem in terms of an inverse Laplace transform. We delay such a study to a future paper.

2 The Correspondence Principle for Simple Free Vibrations

In this section we apply the correspondence principle (1.1) to obtain the torsional modes of a viscoelastic rod. We then show that in a stratified viscoelastic medium in which the anelasticity depends on depth in a certain special way, the correspondence principle (1.1) may be extended to the modes for Love waves. Finally, the section concludes with implementations of (1.1) for for four viscoelastic models. Thus, this section serves as a foundation for the rest of the paper, where these models are discussed in detail.

The torsional modes for an elastic rod may be determined as given by Achenbach (1975). Let the rod have radius r_0, and let $J_j(z)$, $j=0,1$, denote the Bessel function of the first kind and of order j. Let q be a solution of the frequency equation,

$$(qr_0)J_0(qr_0)-2J_1(qr_0) = 0. \tag{2.1}$$

Then in terms of the wave number k (a real number), the density ρ, and the elastic modulus M_e, the corresponding torsional frequency is given by

$$\omega_e = \beta\sqrt{q^2 + k^2}$$

with

$$\beta^2 = M_e / \rho.$$

In terms of the radial position r, the distance z along the rod, and the time t, the elastic displacement field v_e is given by

$$v_e(r,z,t) = \frac{1}{q}J_1(qr)\exp\{i(kz - \omega_e t)\}.$$

Accordingly, the viscoelastic torsional modes are the obtained by solving (1.1) for ω_v, and the associated displacement field v_v is

$$v_v(r,z,t) = \frac{1}{q}J_1(qr)\exp\{i(kz - \omega_v t)\}.$$

For the viscoelastic Love wave problem in a stratified medium, we have from Majda *et al.* (1985) that

$$\frac{d}{dz}\left[M_v(z,\omega_v)\,\frac{dv_v}{dz}\right] + [\omega_v^2\rho(z) - k^2M_v(z,\omega_v)]v_v = 0, \quad 0 < z < \infty, \tag{2.2}$$

$$\frac{dv_v(0)}{dz} = 0 \text{ and } \lim_{z\to\infty} v_v(z) = 0,$$

where k is real, $M_v(z,\omega_v)$ is the depth-dependent complex shear modulus, and

$\rho(z)$ is the density. In (Majda *et al.* 1985) it was assumed that the complex shear modulus varies continuously with z, but the dependence on ω is quite general, provided that $|M_v - M_e|$ is sufficiently small. Here, we permit M_v and M_e to be piecewise continuous in z, but we impose the condition that the complex shear modulus $M_v(z,\omega_v)$ is related to the real shear modulus $M_e(z)$ in the special way,

$$M_v(z,\omega_v) = M_e(z)A(\omega_v), \tag{2.3}$$

where A is an analytic function. Then a correspondence principle for the stratified Love wave problem may be obtained as follows. We rewrite (2.2) using (2.3) to yield

$$\frac{d}{dz}\left[M_e(z)\,\frac{dv_v}{dz}\right] + \left[\frac{\omega_v^2}{A(\omega_v)}\rho(z) - k^2 M_e(z)\right]v_v = 0. \tag{2.4}$$

The corresponding elastic Love wave equation is

$$\frac{d}{dz}\left[M_e(z)\,\frac{dv_e}{dz}\right] + [\omega_e^2\rho(z) - k^2 M_e(z)]v_e = 0. \tag{2.5}$$

Upon comparing (2.4) with (2.5), we conclude that if v_e is a mode for the elastic Love wave problem, then it is also a mode for the viscoelastic Love wave problem, $v_v = v_e$, and the frequencies are related by

$$\frac{\omega_v^2}{A(\omega_v)} = \omega_e^2. \tag{2.6}$$

The multiplicative decomposition postulate (2.3) restricts the frequency-dependent aspect of the material properties to be independent of depth. This assumption may not be valid for solid earth geophysical applications. It may, however, be a sufficiently good approximation for regional studies.

We remark that this analysis may easily be extended to the case in which the density ρ_v for the viscoelastic solid is a constant multiple of the corresponding density ρ_e for the elastic problem. That is, we could just as well let

$$\rho_v(z) = b_v\tilde{\rho}(z), \quad \rho_e(z) = b_e\tilde{\rho}(z),$$

where $\tilde{\rho}(z)$ is a normalized, dimensionless density and b_v and b_e are constants. This change merely causes the introduction of a scaling factor in (2.6).

For both cases (1.1) and (2.6) the problem of calculating the viscoelastic free vibrations reduces to a study of conformal transformations between complex planes. In fact, with the notation

$$s = i\omega_v$$

Eq. (2.6) takes the form

$$f(s) = s\sqrt{\frac{1}{A(-is)}} = i\omega_e \tag{2.7}$$

In (2.7) it is advantageous to continue ω_e onto the complex plane. Thus, we regard $f(s)$ as a map from the complex s-plane into the complex ω_e-plane. Since the elastic modes ω_e are strictly real and are presumed known, it is the inverse transformation f^{-1} that is of interest. In particular, the correspondence principle amounts to finding the curve Γ in the s-plane, which is the image of the real line in the ω_e-plane. In subsequent sections we determine Γ for a Kelvin-Voigt solid, a Maxwell solid, a Standard Linear solid and an Achenbach-Chao model solid. The mapping f^{-1} in each case is multivalued. We shall see that the branches of the multivalued map play an important role.

The complex moduli for these model solids are determined from the dynamic equations for the velocity u and strain tensor ε,

$$\rho \frac{\partial u}{\partial t} = \text{div}\, \sigma. \tag{2.8}$$

$$\frac{\partial \varepsilon}{\partial t} = \frac{1}{2}(\nabla u + (\nabla u)^T), \tag{2.9}$$

where σ is the stress tensor and A^T denotes the transpose of the tensor A. Different viscoelastic models are obtained, depending on the particular constitutive relation, describing the relationship between σ and ε.

1). For a Kelvin-Voigt solid (Leitman & Fisher 1973)

$$\sigma = M_I(\frac{\partial \varepsilon}{\partial t} + \frac{\varepsilon}{\tau_\varepsilon}), \tag{2.10}$$

where M_I is the instantaneous modulus and τ_ε is the stress relaxation time. Thus, for a Kelvin-Voigt solid we find by taking a Laplace transform with respect to t that

$$A(-is) = 1 + s\tau_\varepsilon. \tag{2.11}$$

2). For a Maxwell solid (Leitman & Fisher 1973)

$$\frac{\partial \sigma}{\partial t} + \frac{\sigma}{\tau_\sigma} = M_I \frac{\partial \varepsilon}{\partial t},$$

where τ_σ is the strain relaxation time. Thus, for a Maxwell solid we have

$$A(-is) = \frac{s}{s + \frac{1}{\tau_\sigma}}. \tag{2.12}$$

3). For a standard linear solid (Leitman & Fisher 1973)

$$\frac{\partial \sigma}{\partial t} + \frac{\sigma}{\tau_\sigma} = M_I(\frac{\partial \varepsilon}{\partial t} + \frac{\varepsilon}{\tau_\varepsilon})$$

with $\tau_\sigma < \tau_\varepsilon$. Thus, for a standard linear solid we have

$$A(-is) = \frac{s + \frac{1}{\tau_\varepsilon}}{s + \frac{1}{\tau_\sigma}}. \tag{2.13}$$

4). For an Achenbach-Chao model solid (Achenbach & Chao 1962)

$$(\frac{\partial}{\partial t} + \frac{1}{\tau_\sigma})^2 \sigma = M_I(\frac{\partial}{\partial t} + \frac{1}{\tau_\varepsilon})^2 \varepsilon$$

with $\tau_\sigma < \tau_\varepsilon$. Thus, for an Achenbach-Chao solid we have

$$A(-is) = \left(\frac{\tau_\sigma s + \alpha}{\tau_\sigma s + 1}\right)^2, \qquad 0 < \alpha = \frac{\tau_\sigma}{\tau_\varepsilon} < 1. \tag{2.14}$$

3 Kelvin-Voigt solid

Upon introducing the dimensionless variables

$$p = \tau_\varepsilon s \quad \text{and} \quad \zeta = \tau_\varepsilon \omega_\varepsilon / 2$$

into (2.11), we obtain for the correspondence relation (2.7)

$$\frac{-ip}{2\sqrt{1+p}} = \zeta \tag{3.1}$$

Note that the map (3.1) requires two sheets in the p-plane because of the presence of the square root. In fact, it is clear by inspection that $p=-1$ and $p=\infty$ are branch points. We have to join these two branch points with a cut, and we shall see that the cut is to be taken from $p=-1$ to $p=\infty$ along the negative real axis. The question which is more interest to us, however, is the location of singularities in the ζ-plane, because our task is the determination of the location of the image in the p-plane of the real axis in the ζ-plane. To solve that problem, we may proceed in either of two ways: by analyzing (3.1) directly, or by looking for simpler intermediate transformations. We shall do it both ways, starting with a chain of intermediate transformations.

An inspection of (3.1) suggests the following sequence of transformations. With

$$p = z^2-1 \tag{3.2}$$

Eq. (3.1) becomes the well-known Joukowsky transformation (Bieberbach 1953)

$$\frac{1}{2}\left(z - \frac{1}{z}\right) = i\zeta \tag{3.3}$$

This transformation is also discussed in Appendix A. The map (3.3) may be inverted,

$$z = i\zeta + \sqrt{1-\zeta^2} \tag{3.4}$$

We see that there are branch points at $\zeta=\pm 1$. Note that the inverse function to (3.1) is a composition of (3.4) with (3.2) and that the mapping (3.2) preserves the singularities in (3.4) and adds no new ones. Thus, we need concern ourselves only with the branch points $\zeta=\pm 1$.

We have to use physical principles to determine the location of the cut and to specify the sheet for the mapping (3.4). For ζ on the interval $-1<\zeta<1$, the form of (3.4) suggests the substitution $\zeta=\sin\vartheta$, $-\pi/2\le\vartheta\le\pi/2$. The two corresponding values of z and p are

$$z = e^{i\vartheta}, \quad p = e^{2i\vartheta} - 1, \tag{3.5}$$

$$z = -e^{-i\vartheta}, \quad p = e^{-2i\vartheta} - 1. \tag{3.6}$$

In both cases p goes around the circle of radius 1 with center at -1, as ϑ goes from $-\pi/2$ to $\pi/2$, but the direction is different. In order for (3.1) to be a perturbation of the elastic case $p=i\zeta$ for values of $\zeta\approx 0$, we must choose the counterclockwise branch (3.5). In Fig. 1 the curve (3.5) is shown as a solid curve and (3.6) as a dashed curve.

For ζ on the real axis and $\zeta>1$, the form of (3.4) suggests the substitution $\zeta=\cosh\vartheta$, $0<\vartheta<\infty$, which gives

$$z = ie^{\vartheta}, \quad p = -1 - e^{2\vartheta}, \tag{3.7}$$

$$z = ie^{-\vartheta}, \quad p = -1 - e^{-2\vartheta}, \tag{3.8}$$

For a Kelvin-Voigt solid the dynamic equation (2.8)-(2.10) is of parabolic type, so that $\mathrm{Re}\,p\to-\infty$ as $\zeta\to\infty$ through real values. Consequently, we must choose the branch (3.7). This implies that as ζ passes $\zeta=1$ in the increasing direction on the real axis, the image in the p-plane makes a 90° right turn. Consequently, the cut leaving the branch point $\zeta=1$ must lie in the upper halfplane. In fact, the entire cut from $\zeta=-1$ to $\zeta=1$ must lie in the upper halfplane, for otherwise, the locus of the viscoelastic modes would have a discontinuity.

We still have to determine the image of the part of the real ζ axis from Re $\zeta=-\infty$ to $\zeta=-1$. An analysis similar to that given for (3.7) and (3.8) shows that if we set $\zeta=-\cosh\vartheta$, $0<\vartheta<\infty$, in (3.4), then the proper branch is

$$z = -ie^{\vartheta}, \quad p = -1 - e^{2\vartheta}. \tag{3.9}$$

The complete proper image in the p-plane of the real axis in the ζ-plane is shown as the solid curve in Fig. 1. The extraneous branch (3.8) is drawn with dashes. We conclude by noting that Fig. 1 shows that the cut in the p-plane for the square root in (3.1) is to be taken from $p=-1$ to $p=\infty$ along the negative real axis.

The other approach is to get as much information as possible directly from (3.1). We begin by differentiating (3.1),

$$\frac{d\zeta}{dp} = \frac{-i(p+2)}{4(p+1)^{3/2}} \tag{3.10}$$

The mapping (3.1) fails to be conformal at any point where $d\zeta/dp$ is zero or does not exist. It is clear that these are the points $p=-1$, $p=-2$, and $p=\infty$. Let us begin by examining (3.1) for p near -1. It is clear that $p=-1$ maps onto $\zeta=\infty$, and it follows from (3.1) that the Laurent expansion for p about $\zeta=\infty$ is of the form

$$p = -1 - \frac{1}{4\zeta^2} + O\left(\frac{1}{\zeta^4}\right). \tag{3.11}$$

Consequently, for $\zeta=Re^{i\vartheta}$ with R large,

$$p \approx -1 - \frac{e^{-2i\vartheta}}{4R^2},$$

so that an angle at $p=-1$ is twice the size of the corresponding angle at $\zeta=\infty$. This is the reason for the U-turn at $p=-1$ in the dashed curve in Fig. 1.

At $p=2$ it is clear from (3.10) that $dp/d\zeta$ fails to exist, and the transformation inverse to (3.1) has singularities at the image points $\zeta=\pm1$. In order to determine the type of singularity at, say, $\zeta=1$, we make a Taylor expansion of (3.10) about $p=-2$, taking the branch for which $\sqrt{p+1}=i$ at $p=-2$,

$$\frac{d\zeta}{dp} = \frac{1}{4}(p+2) + O(|p+2|^2).$$

Integration of this approximation shows that

$$\zeta = 1 + \frac{1}{8}(p+2)^2 + O(|p+2|^3)$$

for p in a neighborhood of -2. Thus, for $\zeta=1+re^{i\vartheta}$ with r small, we have

$$p = -2 + \sqrt{8r}e^{i\vartheta/2} + O(r).$$

This shows that an angle at $\zeta=1$ is mapped into an angle at $p=-2$ of half the size, thus explaining the right angles at $p=-2$ in Fig. 1. A similar analysis could be performed to show that there is another square-root singularity at $\zeta=-1$.

It remains to examine the case of $p\to\infty$. It follows directly from (3.1) that

$$p = -4\zeta^2 + O(1) \quad \text{as} \quad \zeta \to \infty, \tag{3.12}$$

and we see again that an angle at $\zeta=\infty$ is doubled in size at $p=\infty$, this time on the other sheet.

We have seen that a simple analysis explains the sharp bends in the curves in Fig. 1, thus giving an understanding of the local behavior near critical points. To get the curves in Fig. 1 away from the critical points, we had to look at the

global picture through the mappings (3.2) and (3.4). These ideas are important to our later discussion of the standard linear solid, because for it we can't construct a simple chain of transformations, and we use the computer to fill in the image curves between the critical points.

We conclude this section by returning to the physical variables. Let

$$\chi = \frac{\tau_\varepsilon \kappa \omega_\theta}{2}$$

Then we have shown that the viscoelastic frequencies of a Kelvin-Voigt solid are given by the following. For $0 < \chi \leq 1$,

$$s = -\frac{1}{\tau_\varepsilon}(1 - \exp\{i 2\sin^{-1}\chi\}). \tag{3.13}$$

and for $1 < \chi < \infty$,

$$s = -\frac{2}{\tau_\varepsilon}\chi^2\left(1 + \sqrt{1 - \frac{1}{\chi^2}}\right) \tag{3.14}$$

The viscoelastic modes of a Kelvin-Voigt solid are analogous to the motions of a damped oscillator, in that, (3.13) represents an underdamped oscillation and (3.14) is a overdamped motion. Critical damping occurs at $\tau_\varepsilon \kappa \omega_\theta = 2$ or $\chi = 1$.

4 Maxwell Solid

For the Maxwell solid (2.12) we introduce the dimensionless variables

$$p = \tau_\sigma s \quad \text{and} \quad \zeta = 2\tau_\sigma \omega_\theta ,$$

and the correspondence relation (2.7) takes the form

$$-2i\sqrt{p(p+1)} = \zeta \tag{4.1}$$

We see immediately that there are branch points at $p=0$ and $p=-1$. Again, we may either analyze (4.1) directly or construct a sequence of simpler transformations. One such sequence is as follows. Let

$$\zeta = -2i\sqrt{w} ,$$

$$w = \xi^2 - \frac{1}{4} ,$$

and

$$\xi = p + \frac{1}{2}$$

Since we are interested in the inverse function to (4.1), we invert these transformations and analyze

$$w = -\frac{\zeta^2}{4} , \tag{4.2}$$

$$\xi = \sqrt{w + \frac{1}{4}} \tag{4.3}$$

$$p = \xi - \frac{1}{2} \tag{4.4}$$

It is clear that the mapping (4.2) has no singularities. The mapping (4.3) has a branch point at $w=-1/4$, which is the image of the points $\zeta=\pm 1$. The

mapping (4.4) is just a translation and has no singularities. Thus, the only singularities for the inverse transformation to (4.1) are branch points of square-root type at $\zeta=\pm 1$.

Let us now determine the image of the real line in the ζ-plane. It is clear that the transformation (4.2) maps the real axis of the ζ-plane onto the negative real axis of the w-plane. For w real and $-1/4 \le w \le 0$, we see from (4.3) and (4.4) that ξ and p are real and that, depending on the branch of the square root, either

$$0 \le \xi \le \frac{1}{2}, \quad -\frac{1}{2} \le p \le 0, \tag{4.5}$$

or

$$-\frac{1}{2} \le \xi \le 0, \quad -1 \le p \le -\frac{1}{2}. \tag{4.6}$$

These are the two images of the real segment $-1 \le \zeta \le 1$. For w real with $w < -1/4$, we see that ξ is purely imaginary, with the two branches complex conjugate of each other. Consequently, the part of the real ζ axis with $|\zeta| \ge 1$ maps onto the line $\mathrm{Re}\, p = -1/2$. The choice of the branch is determined as follows. Let us start with ζ real and $\zeta \approx \infty$. Then in order for high-frequency modes in the Maxwell solid to behave like damped high-frequency elastic modes, we must have $p \approx i\zeta$ as $\zeta \to \infty$. Thus, the segment $-\infty < \zeta < -1$, ζ real, is mapped onto the part of the line $\mathrm{Re}\, p = -1/2$ which lies in the third quadrant. Likewise, the segment $1 < \zeta < \infty$, ζ real, is mapped onto the part of the line $\mathrm{Re}\, p = -1/2$ which lies in the second quadrant. Since there must be no damping in the zero-frequency limit, the branch (4.6) is extraneous, and we must choose the branch (4.5). The full image is shown in Fig. 2. Just as for the Kelvin-Voigt solid, we see by the angles at the corners that the cut from $\zeta=-1$ to $\zeta=1$ must lie in the upper half of the ζ-plane.

As we did for the Kelvin-Voigt solid, we can get a great deal of qualitative information about the inverse to (4.1) by analyzing the behavior of (4.1) near critical points. We begin by differentiating (4.1) to get

$$\frac{d\zeta}{dp} = \frac{-i(2p+1)}{\sqrt{p(p+1)}}.$$

Thus, we see that $d\zeta/dp = 0$ at $p=-1/2$, and $d\zeta/dp = \infty$ at $p=0$ or $p=-1$. The mapping (4.1) is regular at $p=\infty$. Let us examine first the behavior near $p=-1/2$, which by (4.1) corresponds to $\zeta=\pm 1$. Just as for the Kelvin-Voigt solid, we expand $d\zeta/dp$ in a Taylor series about the critical point,

$$\frac{d\zeta}{dp} = -4\left(p + \frac{1}{2}\right) + O\left(\left|p + \frac{1}{2}\right|^2\right). \tag{4.7}$$

Upon integrating (4.7), we see that for $p = -1/2 + re^{i\vartheta}$, we have

$$\zeta + 1 = -2r^2 e^{2i\vartheta} + O(r^3),$$

so that angles at the branch points $\zeta=\pm 1$ are mapped into angles of half the size at $p=-1/2$. Similarly, expansions of (4.1) about $p=0$ and $p=-1$ show that an angle at $\zeta=0$ is mapped into an angle twice the size at $p=0$ or at $p=-1$.

Finally, we transform back to the physical variables to find that the viscoelastic frequencies of a Maxwell solid are given by

$$s = \frac{-1}{2\tau_\sigma}\left[1 - \sqrt{1-\chi^2}\right] \quad \text{for} \quad 0 < \omega_e \le \frac{1}{2\kappa\tau_c}, \tag{4.8}$$

and

$$s = \frac{-1}{2\tau_\sigma}[1 - i\sqrt{\chi^2 - 1}] \quad \text{for} \quad \omega_\varepsilon > \frac{1}{2\kappa\tau_\sigma}, \tag{4.9}$$

where $\chi = 2\kappa\tau_\sigma\omega_\varepsilon$. For frequencies $-1/(2\kappa\tau_\sigma) \le \omega_\varepsilon < 0$, the formula (4.8) remains valid, and for $\omega < -1/(2\kappa\tau_\sigma)$ the viscoelastic modes s are obtained by taking the complex conjugate of (4.9).

It is interesting to note that the Maxwell solid doesn't have the low-frequency, weakly damped free vibrations of the Kelvin-Voigt solid. In the Maxwell solid, there are two distinct sets of vibrations, namely, an oscillatory motion with a fixed decay rate (4.9) and a strictly decaying motion (4.8).

5 Standard Linear Solid

For the standard linear solid we make a change of variables in (2.13)

$$p = \tau_\sigma s \quad \zeta = \tau_\sigma\omega_\varepsilon \quad \text{and} \quad a = \frac{\tau_\sigma}{\tau_\varepsilon},$$

and the correspondence principle (2.7) becomes

$$-ip\sqrt{\frac{p+1}{p+a}} = \zeta \tag{5.1}$$

It is clear that there are branch points at $p = -1$ and $p = -a$. (Note that $0 < a < 1$ by assumption.) We take the branch cut to be the interval from $p = -1$ to $p = -a$.

We do not try to write (5.1) as a sequence of simpler transformations. As an indication of the difficulties inherent in such a project, note that if we square (5.1) and clear fractions, we obtain a cubic equation in p for each value of ζ. This tells us that there are three sheets in the ζ-plane and that any sequence of transformations equivalent to inverting (5.1) will have to include the solution of a cubic. In Figs. 3-6 for four values of a we show the three images in the p-plane of the real axis in the ζ-plane. The principal branch shown as a solid curve, a choice dictated by the fact that for low frequencies ($\zeta \approx 0$), a standard linear solid behaves like a Kelvin-Voigt solid, and for large frequencies ($\zeta \approx \infty$), it behaves like a Maxwell solid. The rest of this section is devoted to an explanation of these figures.

We begin by obtaining as much local information as possible. First, it follows directly from (5.1) that $p = \infty$ is a regular point. In fact, we find that as $\zeta \to \infty$ one branch of the inverse to (5.1) has Laurent expansion of the form

$$p = i\zeta - \frac{1-a}{2} + O\left(\frac{1}{\zeta}\right). \tag{5.2}$$

We get another branch by taking the complex conjugate. This explains the vertical asymptotes in Figs. 3-6.

Upon differentiating (5.1), we find that

$$\frac{d\zeta}{dp} = \frac{-i(2p^2 + (3a+1)p + 2a)}{(p+1)^{1/2}(p+a)^{3/2}} \tag{5.3}$$

It is clear that $d\zeta/dp = 0$ at the zeros p_1 and p_2 of $2p^2 + (3a+1)p + 2a$ and that $d\zeta/dp = \infty$ at the points $p = -a$ and $p = -1$. An expansion of (5.1) about $p = -1$ shows that angles at $\zeta = 0$ are doubled at $p = -1$. Similarly, an expansion of (5.1) about $p = -a$ shows that on this branch angles at $\zeta = \infty$ are doubled at $p = -a$.

Each of the points

$$p_1 = -\frac{(3a+1)}{4} + \frac{1}{4}\sqrt{(1-a)(1-9a)}, \tag{5.4}$$

$$p_2 = -\frac{(3\alpha+1)}{4} - \frac{1}{4}\sqrt{(1-\alpha)(1-9\alpha)}, \tag{5.5}$$

is the image of two branch points in the ζ-plane. The reason for the multiplicity is that in (5.1) there are two values of ζ for every nonzero finite value of p. In Figs. 3-6 the values of p_1 and p_2 are marked with x's.

We consider three cases, depending on whether the p_j are real and distinct, equal (and real), or complex. We begin with $\alpha = 1/9$ because we want the sheet structure in the ζ-plane to depend continuously on α. For $\alpha = 1/9$ the numerator of (5.3) has a zero of second order at $p = p_1 = p_2$. That is, the Taylor series for $d\zeta/dp$ about $p = p_1$ is of the form

$$\frac{d\zeta}{dp} = \frac{-2i(p-p_1)^2}{(p_1+1)^{1/2}(p_1+\alpha)^{3/2}} + O(|p-p_1|^3).$$

Consequently, the Taylor series for $\zeta(p)$ about $p = p_1$ has the form

$$\zeta = c_0 + c_3(p-p_1)^3 + O(|p-p_1|^4)$$

with $c_3 \neq 0$. In fact, it is easy to see from (5.1) that $c_0 = \pm 1/\sqrt{3}$. Thus, for the inverse function with $\alpha = 1/9$ each of the branch points $\zeta = \pm 1/\sqrt{3}$ is a cube-root singularity. In order to have consistency with a Kelvin-Voigt solid at low frequencies and a Maxwell solid at high frequencies, we see that the cut from $\zeta = -1/\sqrt{3}$ to $\zeta = 1/\sqrt{3}$ must lie above the real axis. The structure of the three sheets in the ζ-plane is shown in Fig. 7 in a cross section taken along the imaginary axis.

For $\alpha = 1/9$ the three images in the p-plane of the real axis in the ζ-plane may be explained as follows (see Fig. 4). As Re ζ starts from $-\infty$, the principal branch starts up the solid path (5.2) in the third quadrant. One extraneous branch is the complex conjugate of this one, and it corresponds to the dashed line on sheet 3 in Fig. 7. (If we start in sheet 1 and go around the branch point in the clockwise direction, we cross the cut from above, winding up on sheet 3. The corresponding angle swept out in the p-plane is $-120°$. The other starts at $p = -\alpha$, and it is the image of the dashed line on sheet 2 in Fig. 7.). As ζ passes the branch point $\zeta = -1/\sqrt{3}$, for each of the branches p executes a 60° right turn (because of the cube root). For the principal branch the path goes around the loop in the counterclockwise direction. At $\zeta = 0$ the three images are $p = 0, 0, -1$. At the branch point $\zeta = 1/\sqrt{3}$ the paths make another 60° turn to the right. The principal path connects with (5.2) as $\zeta \to \infty$. In order to draw Fig. 4, we used this local analysis to determine the behavior at $p = \infty$, 0, p_1, $-\alpha$, and -1, and we used Newton's method and continuation in ζ to find how the local pieces join together.

Let us now examine the complex case $1/9 < \alpha < 1$. In that case the values of p_1 and p_2 in (5.4) and (5.5) are complex conjugates of each other, and it follows from (5.1) that the corresponding branch points in the ζ-plane are located at the vertices of a rectangle with center at the origin and sides parallel to the real and imaginary axes. See Fig. 8. The main step involves showing that

$$\frac{p_1+1}{p_1+\alpha} = \frac{-w}{w^*} = -e^{2i\theta}$$

where

$$w = \sqrt{(1-\alpha)} + i\sqrt{(9\alpha-1)} = re^{i\theta},$$

and w^* denotes the complex conjugate of w. Similarly, we have

$$\frac{p_2+1}{p_2+\alpha} = \frac{-w^*}{w} = -e^{-2i\theta}$$

Thus, with $p=\rho e^{i\varphi}$ in (5.4), the four branch points are $\zeta=\pm\rho e^{\pm i(\varphi+\vartheta)}$. This analysis shows that for $1/9<\alpha<1$ the real axis in the ζ-plane does not hit the branch points. Consequently, the only local analysis we have to take into account is that involving $\zeta\to 0$ and $\zeta\to\infty$, and this is the same as for $\alpha=1/9$. In Figs. 5 and 6 we use the Newton's method and continuation in ζ to join these local pieces to form the global images of the real axis in the ζ-plane.

Note that between Figs. 4 and 5 the principal branch varies continuously with α, while the other branches are discontinuous. This may be accomplished with a continuous sheet structure if the cuts for $1/9<\alpha<1$ are taken as in Fig. 8 with the cross section of the sheets on the imaginary axis as shown in Fig. 9. In Figs. 7 and 9 the principal branch of the real axis is marked with a solid line.

It remains to consider $0<\alpha<1/9$, and we see from (5.4) and (5.5) that p_1 and p_2 are real and that $-1<p_2<p_1<-\alpha$. Consequently, by (5.1) the corresponding values ζ_1 and ζ_2 are also real, and the two values of ζ for each p_j are negatives of each other. We join each of these pairs of branch points with a cut just above the real axis. It is easy to see that each of these branch points is of square-root type, explaining the 90° turns in Fig. 3. Finally, in order for the sheet structure to be continuous as $\alpha\to 1/9$ and consistent with Fig. 3, we see that for $|\mathrm{Re}\,\zeta|<\zeta_1$ the sheets are as in Fig. 7, and for $\zeta_1<|\mathrm{Re}\,\zeta|<\zeta_2$ sheets 1 and 3 cross just above the real axis, while sheet 2 is undisturbed.

From an inspection of Figs. 4-6 we might expect that Γ lies in a strip in the p-plane. This is indeed the case. A precise statement of this result is given in the following theorem, which is proved in Appendix B.

THEOREM 1. *The viscoelastic free vibrations of a standard linear solid with* $0<\alpha<1$ *lie in the strip*

$$\{\, p \mid -\frac{1-\alpha}{2} < \mathrm{Re}\, p < 0 \,\},$$

and for $p\neq 0$ *they are always dissipative, i. e.,* $\mathrm{Re}\, p < 0$.

Remarks. The dissipative nature of the viscoelastic modes is to be expected from the dissipativity principle of Gurtin & Herrera (1965). Note also that the edges of the strip are just what is prescribed by the behavior (5.2) as $\zeta\to\infty$ and by the fact that $p=0$ at $\zeta=0$.

6 Achenbach-Chao Model Solid

In terms of the dimensionless variables

$$p = \tau_\sigma s \quad \text{and} \quad \zeta = \tau_\sigma \omega_e / 2$$

with the Achenbach-Chao complex modulus (2.11) the correspondence relation (2.7) takes the form

$$\frac{-ip(p+1)}{2(p+\alpha)} = \zeta \tag{6.1}$$

with $0<\alpha<1$. The inverse function to (6.1) is the solution of

$$p^2 + (1-2i\zeta)p - 2i\zeta\alpha = 0,$$

and is therefore multi-valued, that is, the Riemann surface of ζ has two sheets.

In order to understand the mapping (6.1) from a global point of view, we write (6.1) as a sequence of simpler mappings. In fact, (6.1) is equivalent to the sequence:

$$z = \frac{p+\alpha}{\sqrt{\alpha(1-\alpha)}}, \tag{6.2}$$

$$\xi = \frac{1}{2}(z - \frac{1}{z}), \tag{6.3}$$

and

$$\zeta = -i(\sqrt{\alpha(1-\alpha)}\xi - \alpha + \frac{1}{2}). \tag{6.4}$$

Eq. (6.2) consists of a translation and a change of scale. Eq. (6.4) performs a scale change, a translation, and a rotation. Eq. (6.3) is the well-known Joukowsky transformation. It appears in the discussion of the Kelvin-Voigt solid and is discussed in Appendix A. Thus, the essential feature of (6.1) is the Joukowsky transformation, describing ideal flow past a circular cylinder. The image of the real ζ axis for α=0.3, 0.5, and 0.7 is shown in Figs. 10-12. In each of these cases the principal branch is shown as a solid curve and the extraneous branch is drawn with dashes. The unusual behavior for α=0.3 may be explained as follows. The inverse mapping to (6.3) is

$$z = \xi + \sqrt{(\xi^2 + 1)},$$

which has branch points at $\xi = \pm i$. Consequently, by (6.4) the branch points in the ζ-plane are located at

$$\zeta = \pm\sqrt{\alpha(1-\alpha)} + (\alpha - \frac{1}{2})i. \tag{6.5}$$

Thus, we see that the branch points cross the real axis of the ζ-plane at $\alpha = 1/2$, which causes the behavior for $\alpha < 1/2$ to be different from that for $\alpha > 1/2$.

In order to understand this phenomenon, let us perform a local analysis, starting with an examination of the high-frequency ($\zeta \to \infty$) and low-frequency ($\zeta \to 0$) limits. It is clear from (6.1) that the two images of $\zeta = \infty$ are $p = \infty$ and $p = -\alpha$. In fact, a slightly more detailed analysis of (6.1) shows that as $\zeta \to \infty$ these two branches have Laurent expansions of the form

$$p = 2i\zeta - (1 - \alpha) + O(\frac{1}{\zeta}) \tag{6.6}$$

and

$$p = -\alpha + \frac{i\alpha(1-\alpha)}{2\zeta} + O(\frac{1}{|\zeta|^2}). \tag{6.7}$$

It is clear that the branch (6.6) is a perturbation of the elastic case $p = 2i\zeta$, while (6.7) is not.

From (6.1) it is evident that the images of $\zeta = 0$ are $p = 0$ and $p = -1$, but only the branch $p = 0$ makes sense physically. Thus, it would seem as if all we have to do is to extend the branch (6.6) until it goes through $p = 0$ at $\zeta = 0$. This turns out to be possible only if $\alpha \geq 1/2$.

It is true that we have already found in (6.5) the locations of the branch points, but alternatively, we could also do this by a local analysis. Upon differentiating (6.1), we see that

$$\frac{d\zeta}{dp} = \frac{p^2 + 2\alpha p + \alpha}{2i(p + \alpha)^2},$$

so that $d\zeta/dp = 0$ and $dp/d\zeta$ fails to exist when p takes on the values

$$p_1 = -\alpha + i\sqrt{\alpha(1-\alpha)},$$

$$p_2 = -\alpha - i\sqrt{\alpha(1-\alpha)}$$

The images of these points are the points (6.5)

$$\zeta_1 = \sqrt{\alpha(1-\alpha)} + (\alpha - \tfrac{1}{2})i \tag{6.8}$$

and

$$\zeta_2 = -\sqrt{\alpha(1-\alpha)} + (\alpha - \tfrac{1}{2})i, \tag{6.9}$$

and it is easy to show that they are branch points of square-root type. We see from (6.8) and (6.9) that ζ_1 and ζ_2 lie on the circle

$$\gamma = \{\zeta: |\zeta| = 1/2\}$$

and that they lie in the upper half of the ζ-plane if $1/2<\alpha<1$ and in the lower half if $0<\alpha<1/2$. This implies that for $\alpha>1/2$ if we connect the branch points by a cut in the upper half plane and if the location of the cut depends continuously on α, then in every neighborhood of $\alpha=1/2$ the image in the p-plane of the real axis in the ζ-plane must have some sort of discontinuity. Either the cut lies completely in the lower half plane for $\alpha<1/2$ resulting in violation of the (6.6) as $\zeta\to\infty$ or of $p=0$ at $\zeta=0$, or the cut crosses the real ζ axis, resulting in breaks in the image curve but maintaining (6.6) as $\zeta\to\infty$ and $p=0$ at $\zeta=0$. In Fig. 10 for $\alpha=0.3$ we have chosen the second option, arbitrarily taking the cut to be the lines Re $\zeta=\pm\sqrt{\alpha(1-\alpha)}$, Im $\zeta\geq\alpha-1/2$. This behavior implies that for $\alpha<1/2$ it is not possible to represent the solution of a dynamic viscoelastic wave problem in terms of modes alone; the contribution of contour integrals around the branch points must also be included.

Acknowledgment

The work of the first and second authors was performed under the auspices of the U. S. Department of Energy by the Lawrence Livermore National Laboratory under Contract No. W-7405-ENG-48

References

Achenbach, J. D., 1975, *Wave Propagation in Elastic Solids*, North-Holland, Amsterdam.

Achenbach, J. D., & Chao, C. C., 1962, A Three-Parameter Viscoelastic Model Particularly Suited for Dynamic Problems, *J. Mech. Phys. Solids*, **10**, 245-252.

Bieberbach, L., 1953, *Conformal Mapping*, Chelsea, New York.

Fisher, G. M. C., & Leitman, M. J., 1966, A Correspondence Principle for Free Vibrations of a Viscoelastic Solid, *ASME Trans. Ser. E J. Appl. Mech.*, **33**, 924-926.

Gurtin, M. E., & Herrera, I., 1965, On Dissipation Inequalities and Linear Viscoelasticity, *Quart. Appl. Math.*, **23**, 235-245.

Kato, T., 1966, *Perturbation Theory for Linear Operators*, Springer-Verlag, New York.

Leitman, M. J., & Fisher, G. M. C., 1973, The Linear Theory of Viscoelasticity, pp. 1-123 in *Handbuch der Physik*, Vol. VIa/3, ed. C. Truesdell, Springer-Verlag, Berlin-Heidelberg-New York.

Majda, G., Chin, R. C. Y., & Followill, F. E., 1985, A Perturbation Theory for Love Waves in Anelastic Media, *Geophys. J. R. astr. Soc.*, **80**, 1-34.

Naimark, M. A., 1968, *Linear Differential Operators*, Vol. 2, Ungar, New York.

Spencer, Jr., J. W., 1981, Stress Relaxations at Low Frequencies in Saturated Rocks: Attenuation and Modulus Dispersion, *J. Geophys. Res.*, **86**, 1803-1812.

Thigpen, L., Hedstrom, G. W., Bonner, B. P., 1983, Inversion of Creep Resoponse for Retardation Spectra and Dynamic Viscoelastic Functions, *ASME Trans. Ser. E J. Appl. Mech.*, **50**, 361-366

Appendix A The Joukowsky Transformation

For the sake of completeness we include here a brief discussion of the Joukowsky transformation

$$w = \frac{1}{2}(z - \frac{1}{z}), \tag{A.1}$$

which we met in our discussion of the Achenbach-Chao model solid in Eq. (6.3) and of the Kelvin-Voigt solid in Eq. (3.3). (Actually, Eq. (3.3) contains an additional factor $-i$ which merely performs a rotation by $-90°$.) Similar analysis of the Joukowsky transformation may be found in classical references on conformal mapping, such as the book by Bieberbach (1953).

We begin by examining the images in the w-plane of circles $z = re^{i\vartheta}$ in the z-plane parameterized by the radius r. We see from a direct substitution that

$$\mathrm{Re}\, w = \frac{1}{2}(r - \frac{1}{r})\cos\vartheta, \quad \mathrm{Im}\, w = \frac{1}{2}(r + \frac{1}{r})\sin\vartheta. \tag{A.2}$$

Thus, the unit circle $z = e^{i\vartheta}$ is collapsed onto the segment from $w = -i$ to $w = i$. In our analysis of the Kelvin-Voigt and Achenbach-Chao solids we actually used the mapping inverse to (A.1). It is for this reason that a circle appears as the image of a line segment in Figs. 1 and 11.

For values of r different from 1 we see from (A.2) that the image in the w-plane is an ellipse centered on the origin with major axis of length $(r + 1/r)/2$ and on the imaginary axis and with minor axis of length $(r - 1/r)/2$. Thus, each of these ellipses has its foci at $w = \pm i$, and the segment we obtained when $r = 1$ is merely a degenerate ellipse of this family. Note that for $r > 1$ the circles in the z-plane of radius r and $1/r$ map onto the same ellipse in the w-plane.

In our discussion of the Achenbach-Chao model solid we were interested not in the inverse images of ellipses, but of lines, Re w = constant. The images in the z-plane of several such lines are shown in Fig. 13. They represent the streamlines of irrotational flow past a circular cylinder, and that is the reason for the classical interest in the mapping. Note in Fig. 13 the special role played by the circle $|z| = 1$, separating the external flow field from the internal flow field. We have seen that the inverse transformation to (A.1) is double valued. This is shown in Fig. 13 by the fact that each line, Re w = constant $\neq 0$, is mapped onto an exterior streamline and an interior streamline. In Fig. 13 one of these images is drawn as a solid curve and the other with dashes. We have chosen rather unusual cuts ($\mathrm{Im}\, w = \pm 1$, $\mathrm{Re}\, w \leq 0$) in keeping with the cuts introduced in Section 6. Thus, the curves shown in Figs. 10-12 are simply individual curves from Fig. 13 with appropriate translation and scaling.

Appendix B Proof of Theorem 1

In this appendix we show by elementary arguments that if $p = x + iy$ with $y \neq 0$ such that (5.1) is satisfied for real ζ, then $-(1-a)/2 < x < 0$. This is equivalent to Theorem 1. We begin by transforming the problem to a question of determining the location of the real zeros of a cubic polynomial in x with coefficients depending on a and y.

If we square both sides of (5.1) and multiply by $-(p+a)(p^*+a)$, we obtain the relation

$$p^2(p + 1)(p^* + a) = -|p + a|^2\zeta^2, \tag{B.1}$$

where $p^* = x - iy$. For ζ real the right-hand side of (B.1) is real. Thus, upon setting the imaginary part of the left-hand side of (B.1) equal to zero with $p = x + iy$, we find that

$$(2x^3 + (1 + 3\alpha)x^2 + 2(\alpha + y^2)x + (1 - \alpha)y^2)y = 0. \qquad (B.2)$$

Note that the right-hand side of (B.1) is real when ζ is pure imaginary, so that (B.2) also contains the images of the imaginary axis in the ζ-plane. In particular, this includes the part of the real axis $y=0$ with $x>-\alpha$ or $x<-1$, as is easily seen from (5.1). In any case, the trivial solution $y=0$ is not of interest to us. Therefore, we are led to the question of locating the zeros of the polynomial in x.

$$f(x) = 2x^3 + (1 + 3\alpha)x^2 + 2(\alpha + y^2)x + (1 - \alpha)y^2. \qquad (B.2)$$

Since $0<\alpha<1$, it is clear from (B.2) that $f(x)>0$ if $x\geq 0$ and $y\neq 0$. Thus, we have shown that the solutions of (5.1) for real ζ lie in the halfplane $\mathrm{Re}\, p\leq 0$ with only the point $p=0$ lying on the boundary.

In order to show that $\mathrm{Re}\, p$ is bounded from below by $-(1-\alpha)/2$ for p on Γ, let us begin by performing a combined shift and reflection in (B.2). Upon setting $x=-z-(1-\alpha)/2$ and

$$g(z) = -f(-z - \frac{1-\alpha}{2}),$$

we find that

$$g(z) = 2z(z - \frac{3\alpha - 1}{2})^2 + 2y^4 z + \alpha^2(1 - \alpha).$$

Thus, it is clear that $g(z)>0$ if $z\geq 0$ and $0<\alpha<1$. In other words, we have shown that $f(x)<0$ if $x\leq -(1-\alpha)/2$. That is, the zeros of f(x) are restricted to lie in the interval $-(1-\alpha)/2<x\leq 0$, and the curve Γ lies in the strip $-(1-\alpha)/2<\mathrm{Re}\, p\leq 0$. This completes the proof of the theorem

List of Figures.

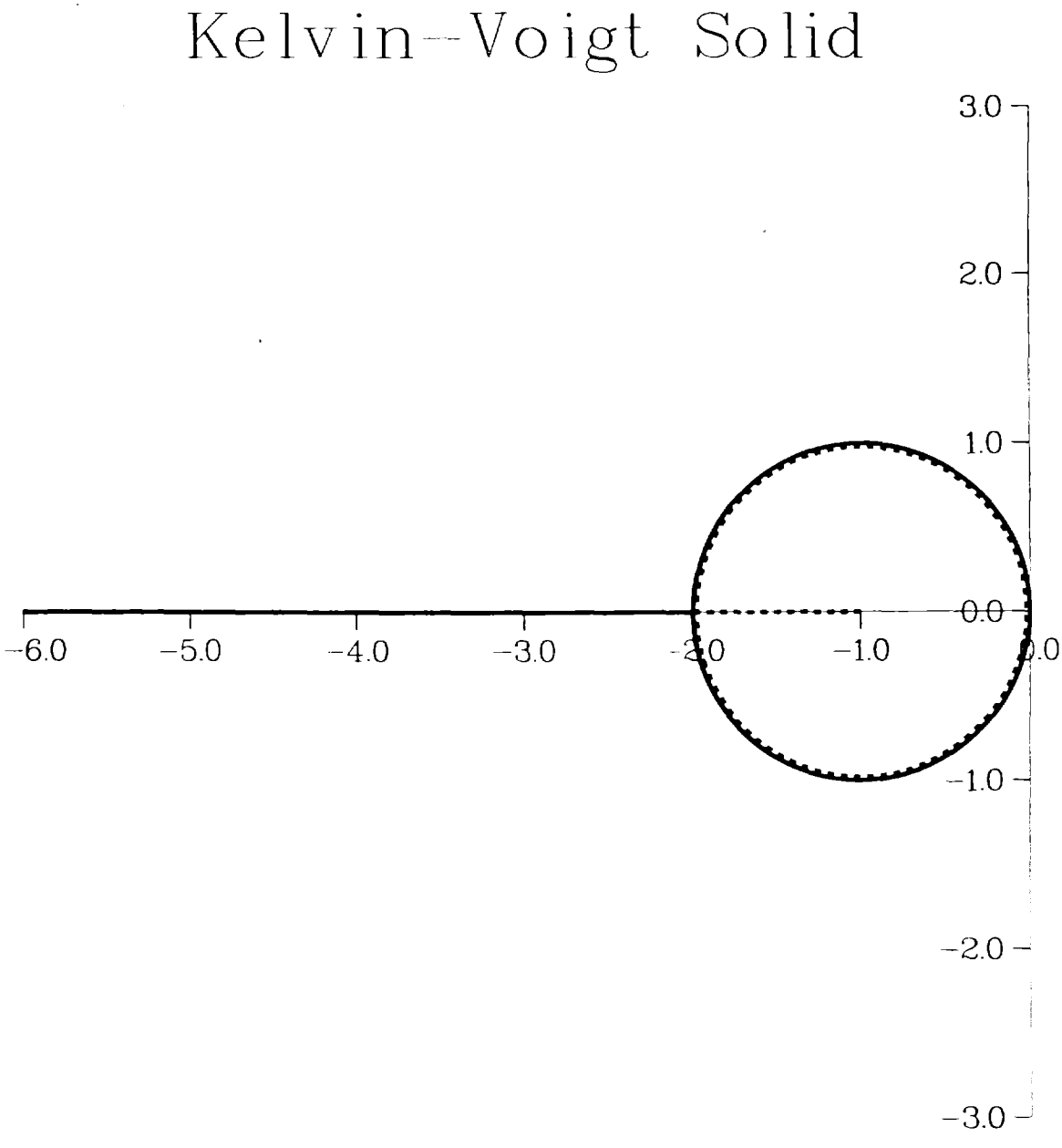

Fig. 1

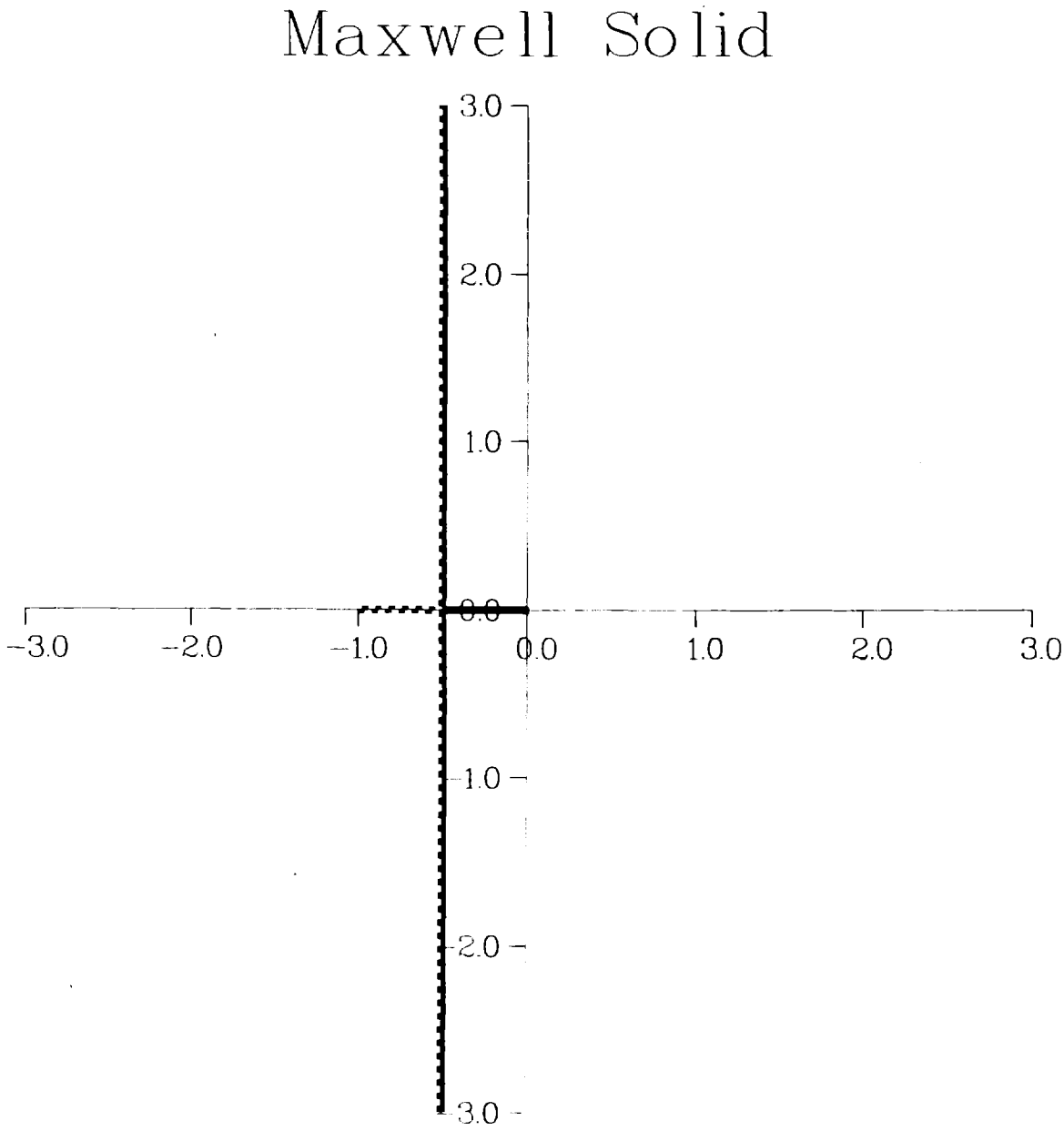

Fig. 2

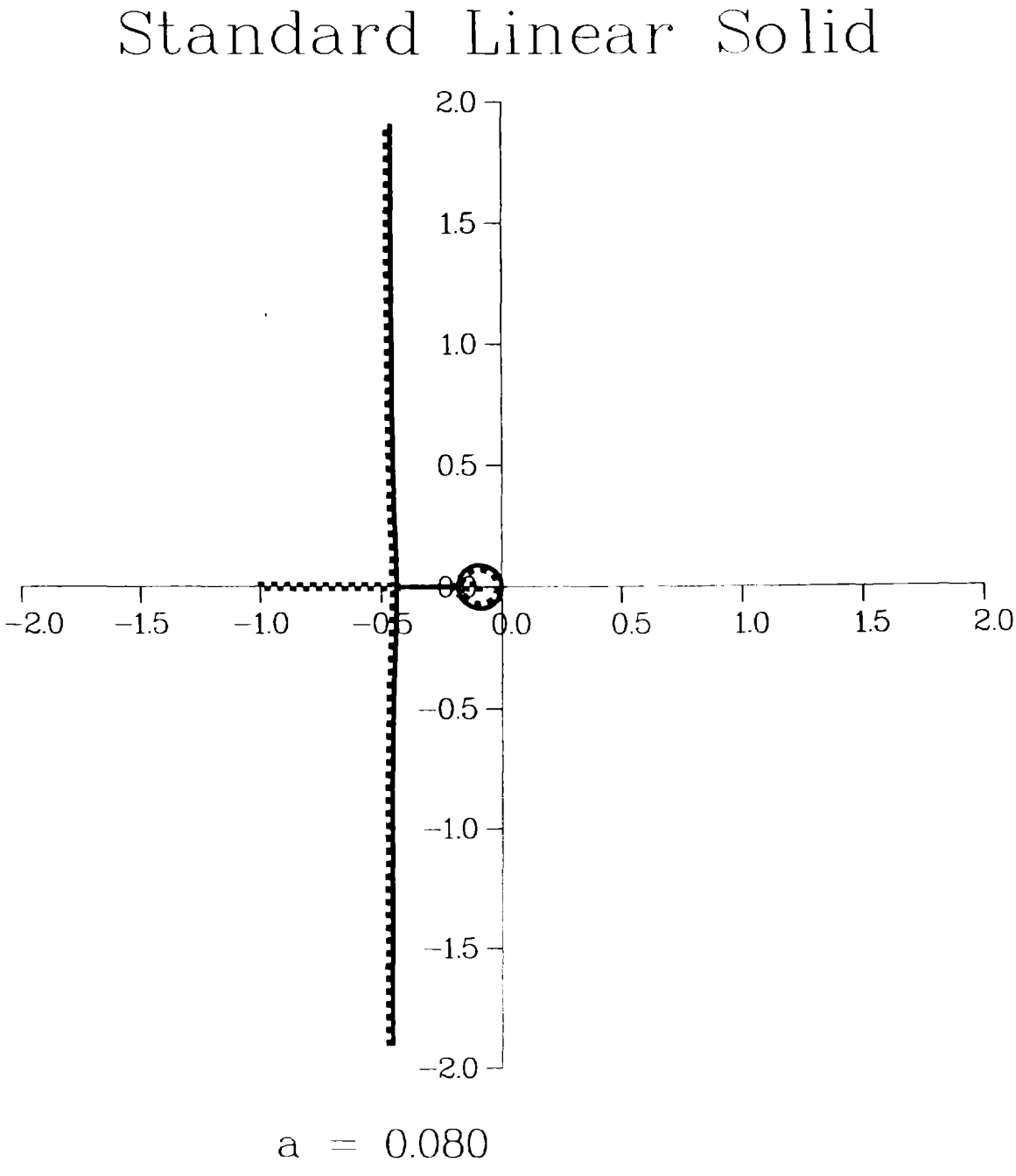
Standard Linear Solid
2.0
1.5
1.0
0.5
0.0
−0.5
−1.0
−1.5
−2.0
−2.0
−1.5
−1.0
0.0
0.5
1.0
1.5
2.0
a = 0.080

Fig. 3

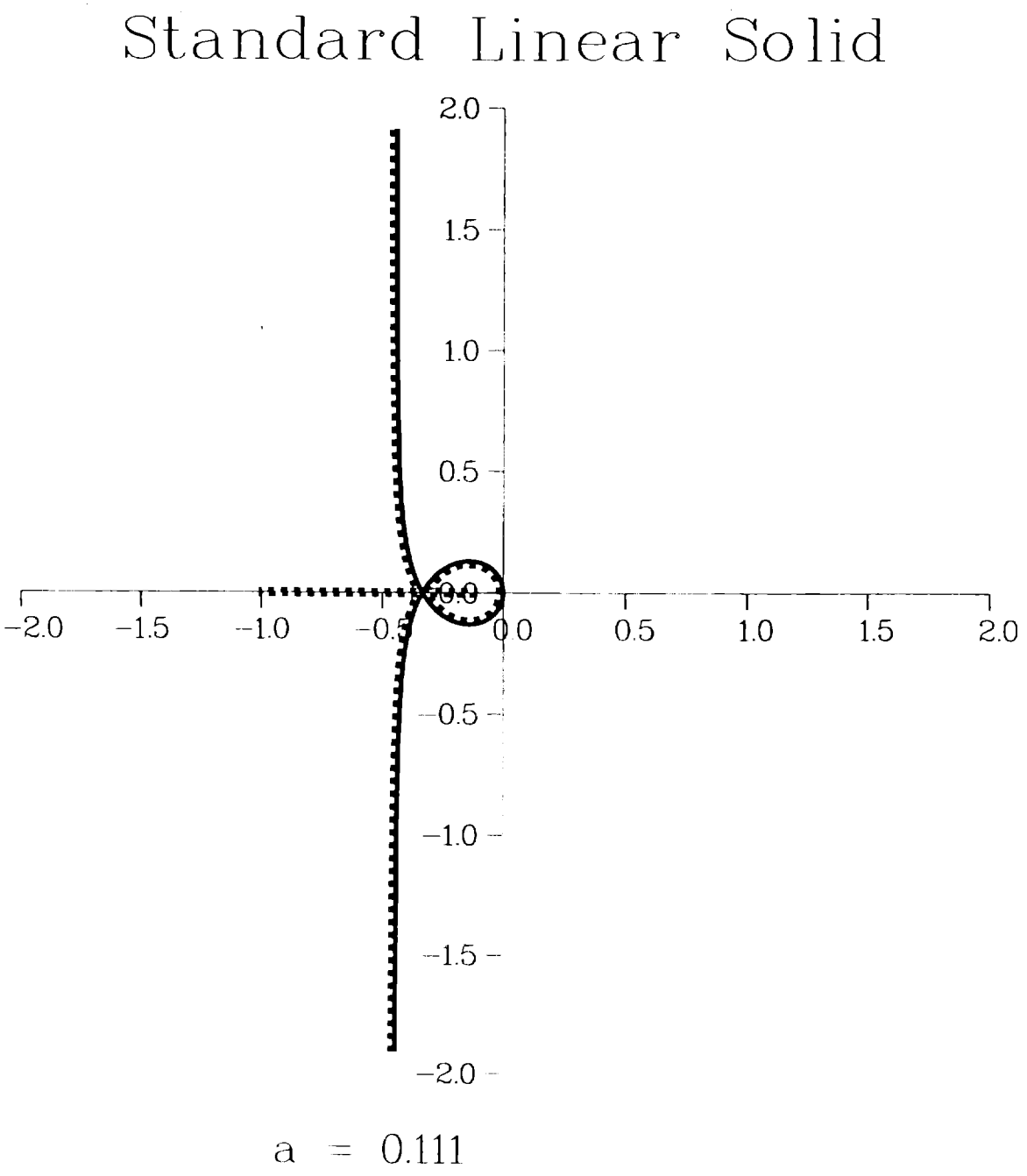
Standard Linear Solid
2.0
1.5
1.0
0.5
0.0
−0.5
−1.0
−1.5
−2.0
−2.0
−1.5
−1.0
−0.5
0.0
0.5
1.0
1.5
2.0
a = 0.111

Fig. 4

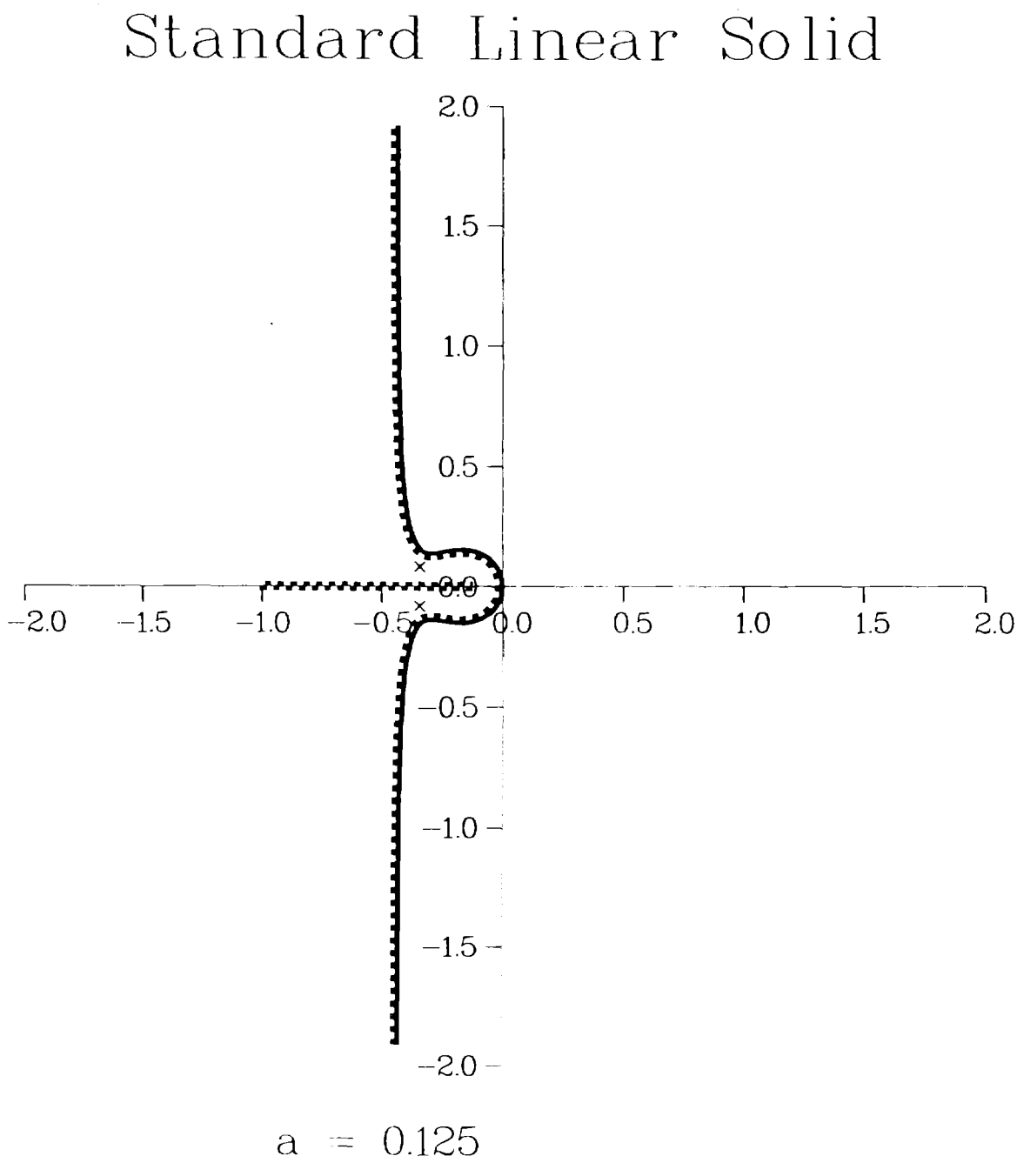
Standard Linear Solid
2.0
1.5
1.0
0.5
0.0
−0.5
−1.0
−1.5
−2.0
−2.0
−1.5
−1.0
−0.5
0.0
0.5
1.0
1.5
2.0
a = 0.125

Fig. 5

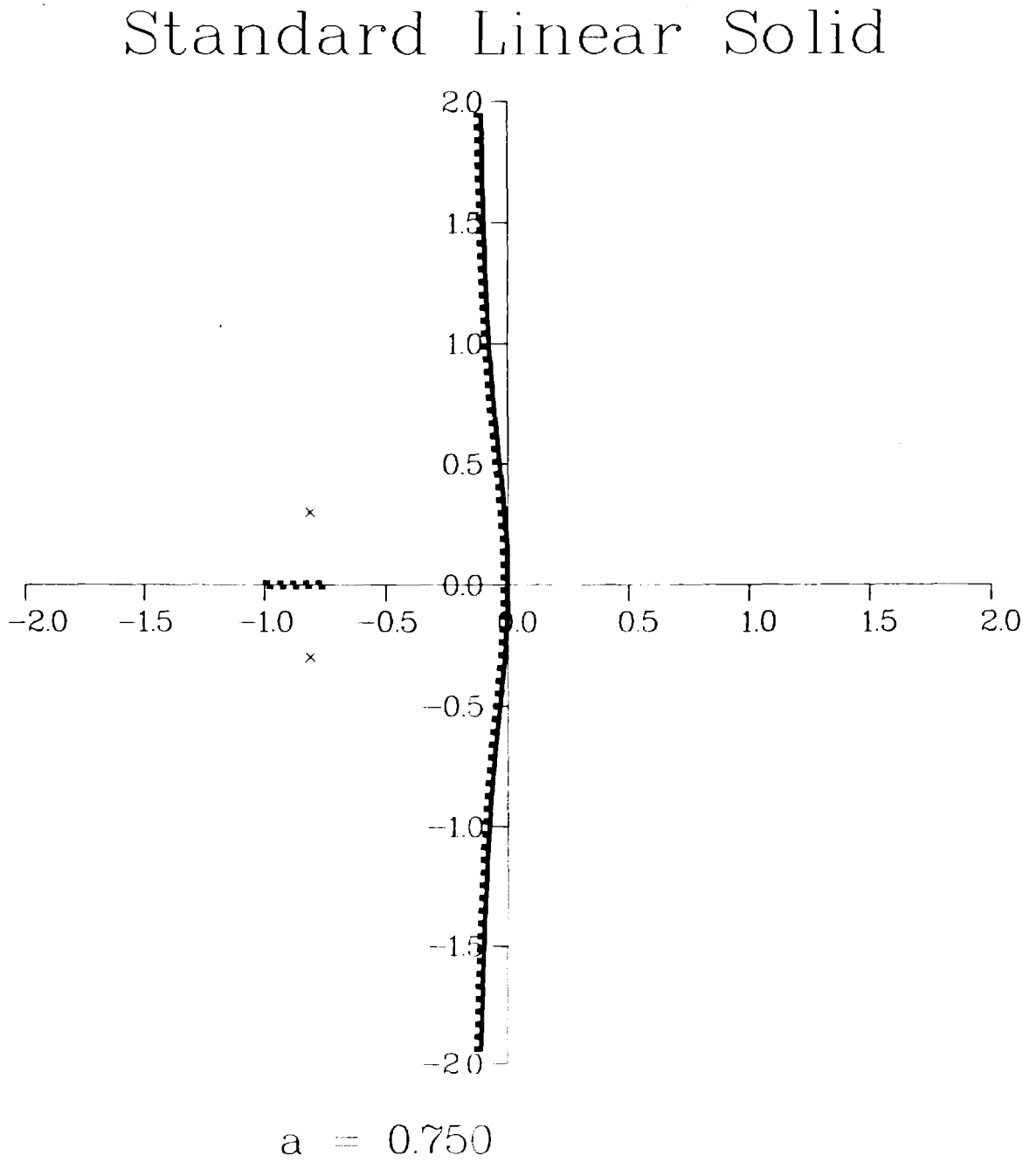
Standard Linear Solid
2.0
1.5
1.0
0.5
0.0
−0.5
−1.0
−1.5
−2.0
−2.0
−1.5
−1.0
−0.5
0.0
0.5
1.0
1.5
2.0
a = 0.750

Fig. 6

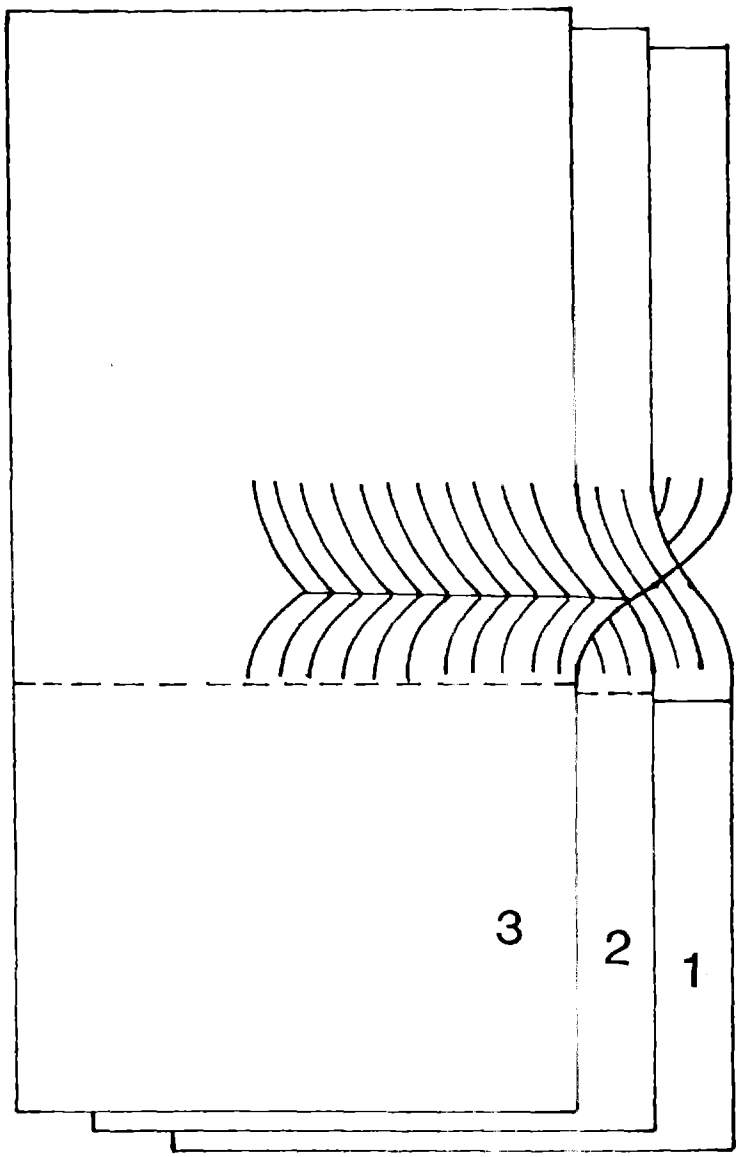

Fig. 7

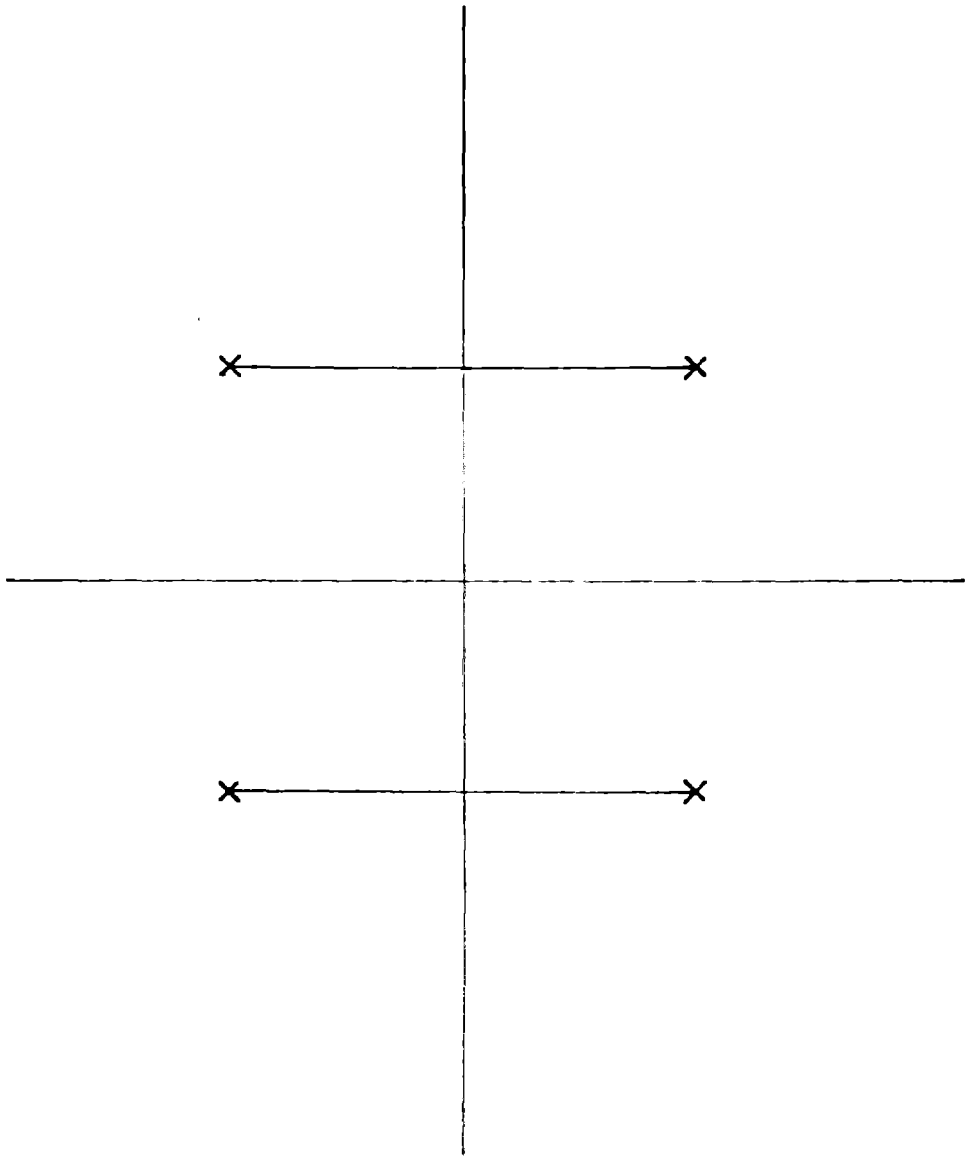

Fig. 8

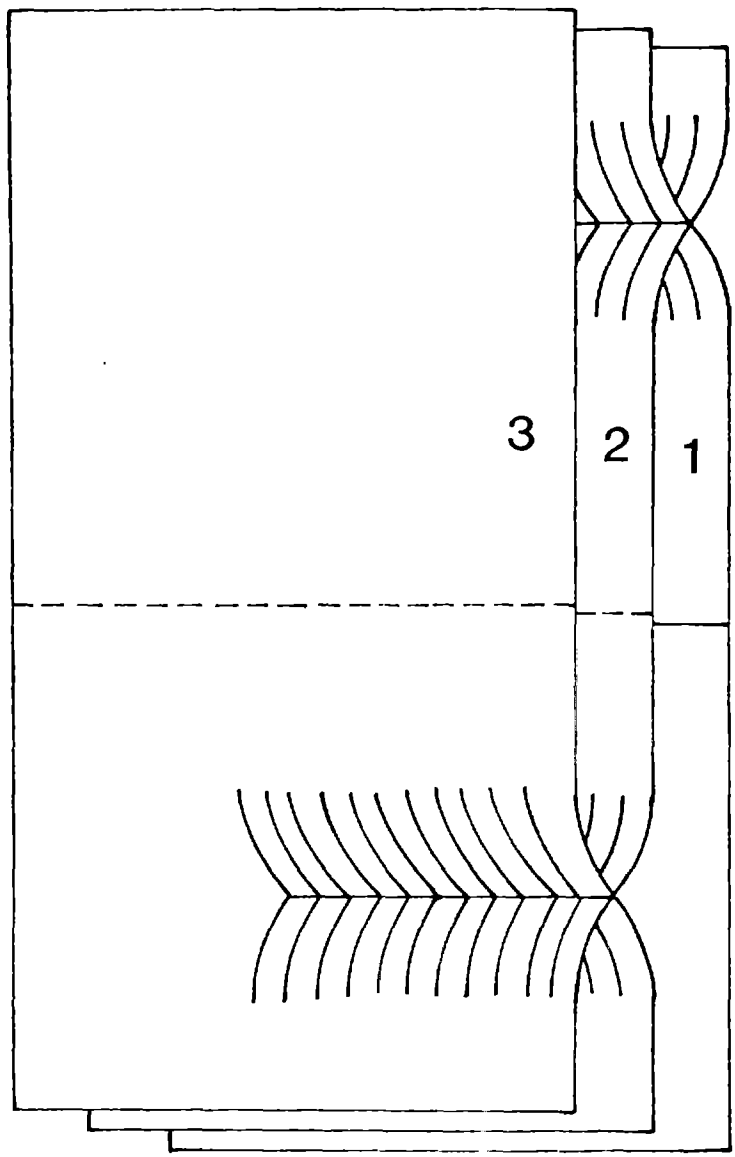

Fig. 9

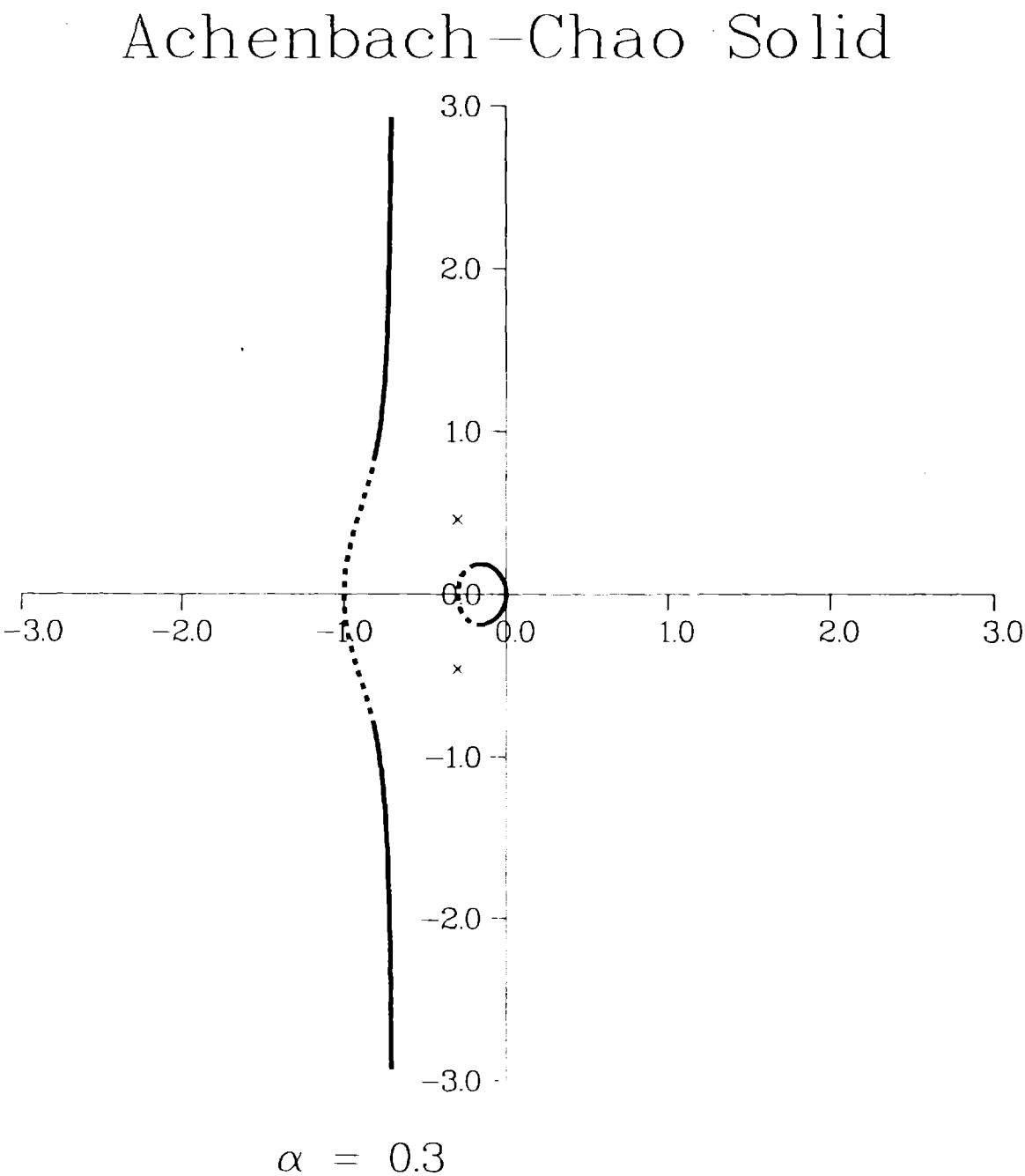

Fig. 10

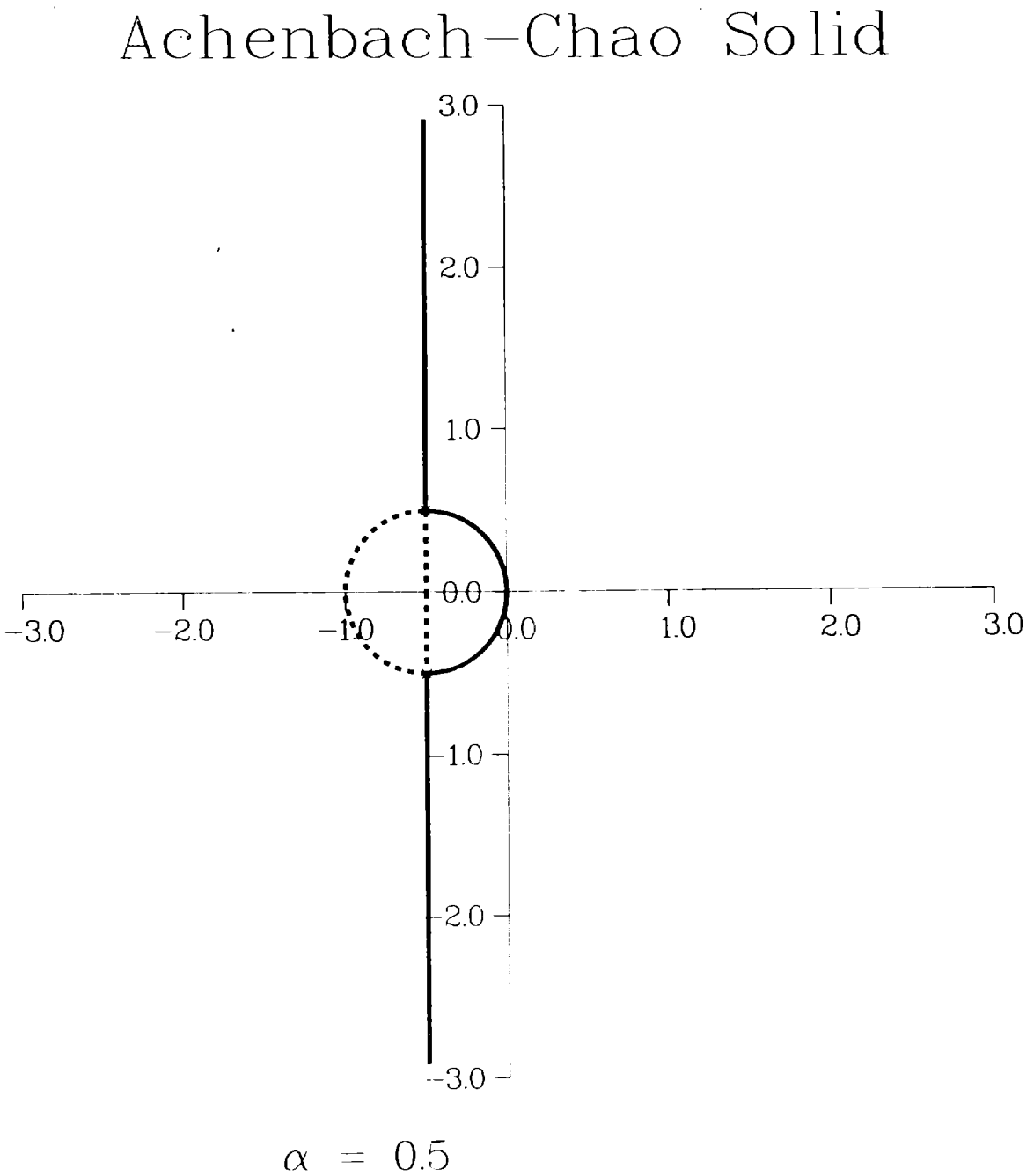

Fig. 11

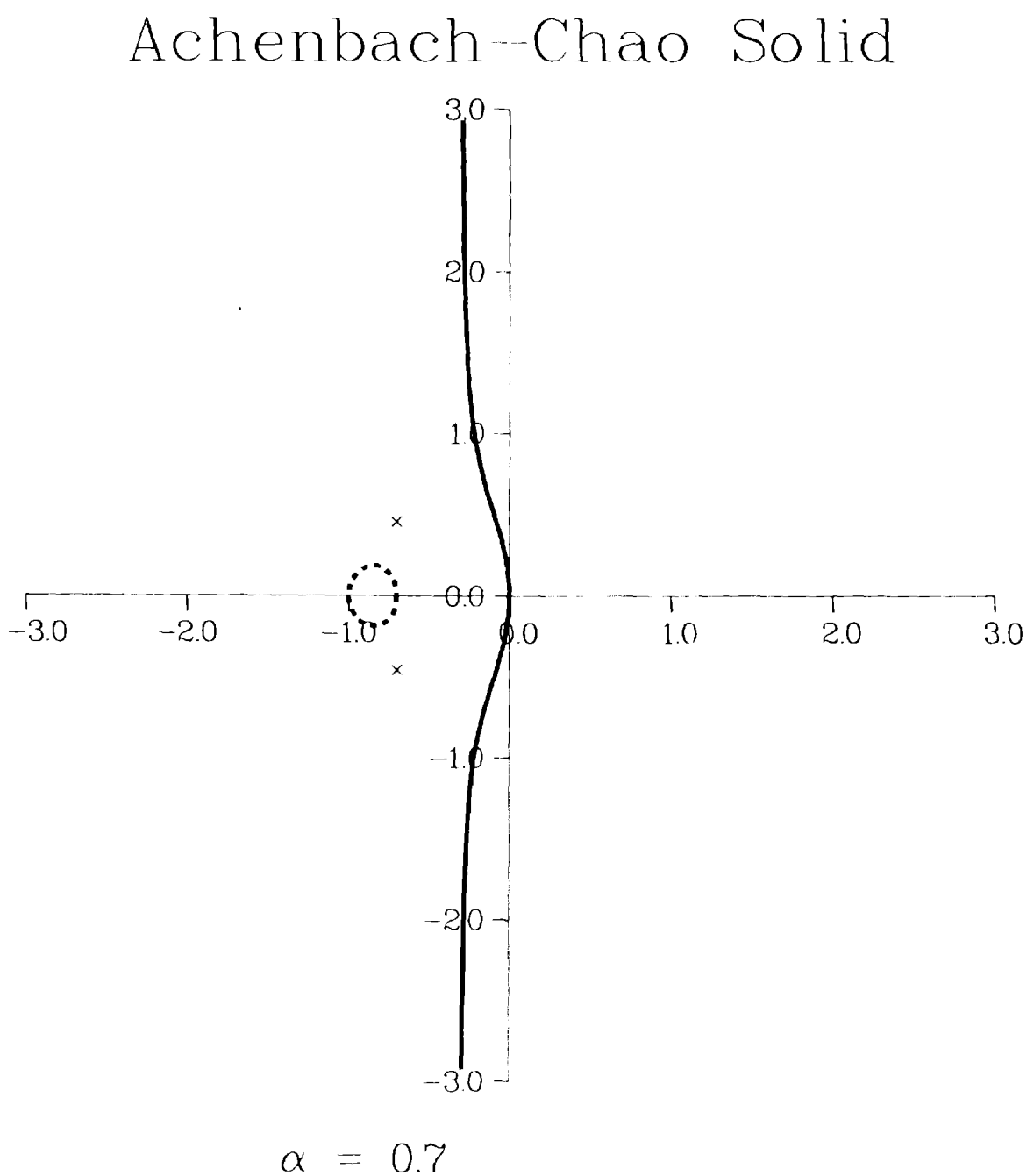

Fig. 12

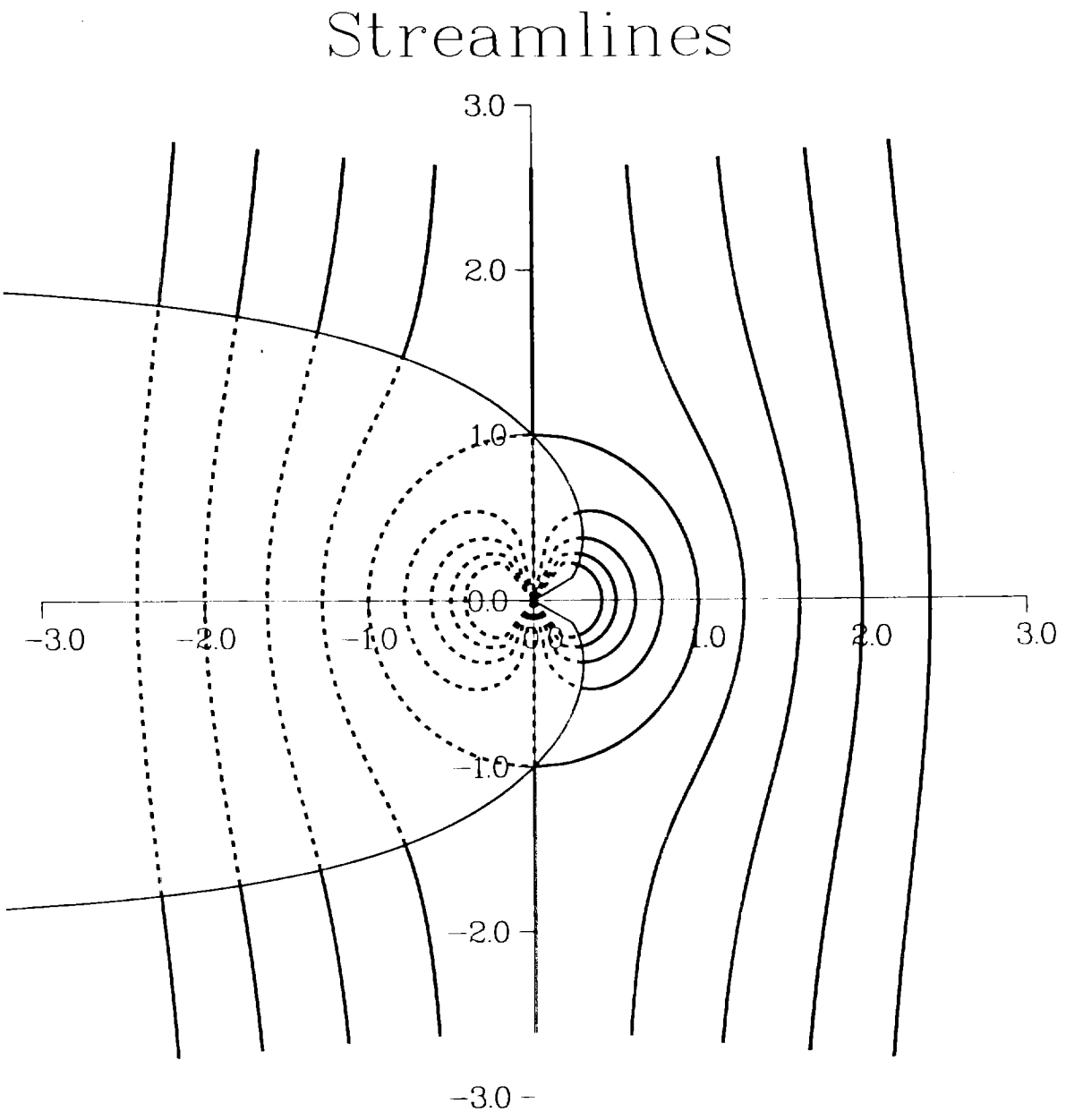

Fig. 13